Broadband, Efficient, and Low Dark Current SiN-on-SOI Waveguide-Coupled Photodetectors for Visible Light

Alperen Govdeli[1,2,†*], Jared C. Mikkelsen[1, †], Abhishek Suriya[1], Hongyao Chua[3], Guo-Qiang Lo[3], Joyce K. S. Poon[1,2], Wesley D. Sacher[1,*]

[1]Max Planck Institute of Microstructure Physics, Weinberg 2, 06120 Halle, Germany
[2]Department of Electrical and Computer Engineering, University of Toronto, 10 King's College Road, Toronto, Ontario M5S 3G4, Canada
[3]Advanced Micro Foundry Pte. Ltd., 11 Science Park Road, Singapore Science Park II, 117685, Singapore
[†]These authors contributed equally to the work.
[*] alperen.govdeli@mail.utoronto.ca, wesley.sacher@mpi-halle.mpg.de

Abstract: We demonstrate foundry-fabricated waveguide-coupled photodetectors wherein silicon nitride waveguides pass overtop doped silicon-on-insulator patches. At a 5V reverse bias, dark currents < 8pA, and red, green, and blue-wavelength external quantum efficiencies >70% were measured. © 2024 The Author(s)

1. Introduction

Leveraging the advancements in silicon (Si) photonics for telecom and datacom, which frequently incorporate silicon nitride (SiN) waveguides [1,2], a number of Si platforms have been developed for the visible spectrum [3-7]. These platforms, produced on 200-mm or 300-mm wafers, employ SiN [6,7] or Al_2O_3 [4] waveguides patterned using deep ultraviolet lithography. To support applications spanning quantum information [8], biophotonics [9], and display [10], active functionality is necessity. Toward this, recent efforts have developed phase shifters [11-13], photodetectors [14-16], and co-packaged lasers [17].

Si's natural ability to absorb visible (VIS) and near-infrared (NIR) light allows for convenient integration of photodetectors (PDs) within existing Si platforms. For example, SiN waveguides end-coupled to Si PDs have been demonstrated with a responsivity of 0.83A/W at a 685nm wavelength [14], while Al_2O_3 waveguides evanescently coupled to Si PDs achieved 0.25A/W at 405 nm [18]. Our prior work introduced PIN and PN PDs based on doped mesas in bulk Si wafers. These PDs, evanescently coupled to SiN waveguides, achieved > 50% external quantum efficiencies (EQEs) at wavelengths ranging from 405-532nm for TE polarized light and > 60% EQE from 405-640 nm for the TM polarization. We also recorded dark currents of 144 ± 42 pA at a 5V reverse bias [15].

Our first-generation (Gen-1) waveguide-coupled Si mesa photodetectors (PDs) were developed on 200-mm bulk Si substrates featuring dual SiN waveguide layers, efficient phase shifters, and MEMS devices [3]. In contrast, our present work introduces our second-generation (Gen-2) PDs fabricated on 200-mm silicon-on-insulator (SOI) substrates. These Gen-2 PDs, featuring a SiN waveguide evanescently coupled to a doped Si patch where either a PIN or PN junction exists (Fig. 1), outperform their Gen-1 counterparts. Specifically, they achieve higher external quantum efficiencies (EQEs) of over 70% across red, green, and blue wavelengths, along with an 18x reduction in dark current (< 8pA at a 5V reverse bias). The current Gen-2 PDs maintain a comparably large optical bandwidth while substantially enhancing EQE and minimizing dark current. Additionally, electrical crosstalk issues present in Gen-1, due to Si mesa coupling, are eliminated in Gen-2 through full-etching of the Si device layer.

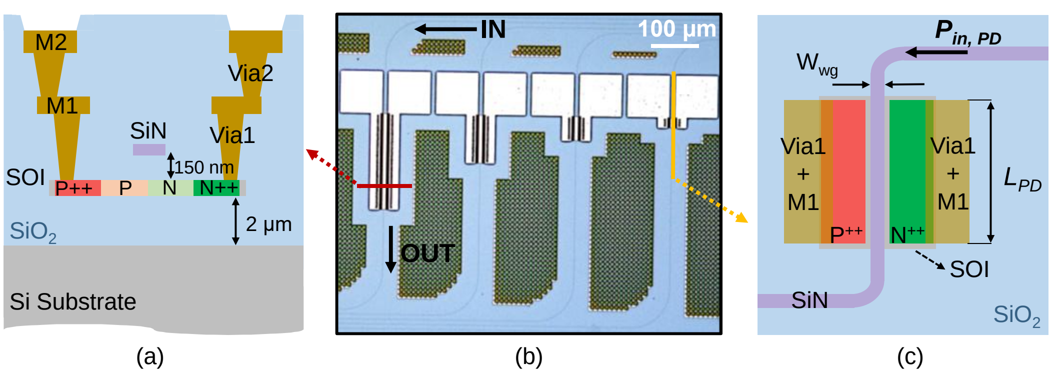

Fig. 1. Visible-light SiN-on-SOI waveguide-coupled PDs. (a) Cross-section schematic of the PDs. (b) Optical micrograph of PDs of different lengths; the brightness and contrast have been adjusted for enhanced visibility of the waveguides. (c) Top-down schematic of the PDs (Via2 and M2 layers not shown). (a) shows the PN variation of the PDs, and (c) shows the PIN variation of the PDs (without the moderately-doped P and N sections).

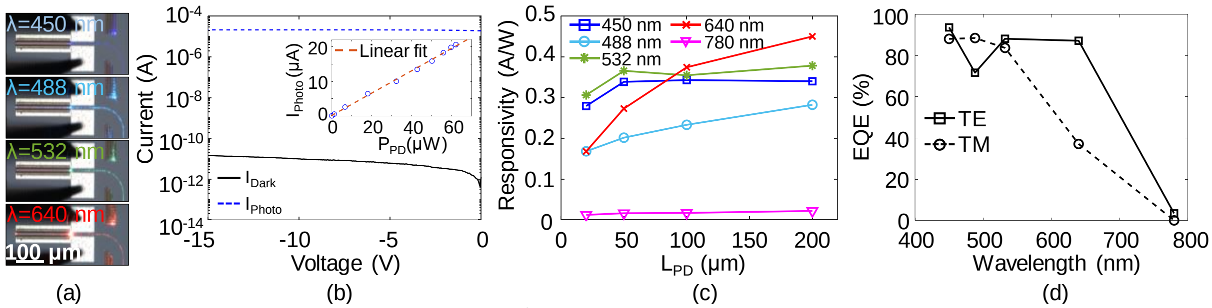

Fig. 2. PIN PD characterization. (a) Optical micrographs of a PD with various visible-wavelength optical inputs. (b) Current-voltage (I-V) traces of a 200μm-long PD with and without input light (λ=450nm, TE-polarized, 61μW incident at the PD). Inset: photocurrent (I_{Photo}) as a function of optical input power to the PD (P_{PD}) for λ=450 nm. Data points (blue circles) and linear fit (red dashed line) with a slope of 0.32 A/W and coefficient of determination, R^2, of 0.99; the slope agrees with the responsivity in (c). (c) Responsivity vs. photodetector length at various wavelengths. (d) EQE vs. wavelength for a 200μm-long PD with TE- and TM-polarized input light.

2. Design, Fabrication, and Characterization

Figure 1(a) illustrates the cross-sectional schematic of the PDs. A 120-nm thick SiN waveguide is positioned above a 220-nm thick Si patch on the SOI wafer. The inter-layer separation is 150 nm, sufficient for efficient evanescent coupling. The design uses heavily-doped (P++ and N++) Si sections for ohmic contacts, which are separated by a 2μm gap. In the PN variant, moderately-doped (P and N) regions form a junction beneath the SiN waveguide. In the PIN junctions, the moderately-doped regions were not implemented. Electrical connectivity is established using two metal layers and two via layers. The PDs are connected to edge couplers through 500-nm wide routing waveguides, and waveguide bends orient the PDs orthogonal to the edge couplers to minimize stray light effects, as shown in Fig. 1(b). Various design parameters including waveguide widths (W_{wg}) of 500 nm and 250 nm, and lengths (L_{PD}) of 20-200 μm were explored.

Vertical optical confinement in the Si patch leads to modal hybridization in the SiN and Si at specific wavelengths, enhancing the absorption per unit length. 3D finite-difference time-domain (FDTD) simulations indicate that an L_{PD} between 100 and 200μm is sufficient for nearly complete absorption in broadband applications, even without modal hybridization. Electrical simulations show that our Gen-2 PDs exhibit significantly reduced dark current compared to Gen-1, likely due to a smaller junction volume under the waveguide.

The Gen-2 visible-light photonics platform was fabricated at Advanced Micro Foundry (AMF) on 200-mm SOI. The Si device layer was patterned and doped via ion implantation and rapid thermal annealing. The SiN waveguide layer was formed with plasma enhanced chemical vapour deposition (PECVD), defined by deep ultraviolet (DUV) photolithography and etched with reactive ion etching (RIE). Chemical mechanical polishing (CMP) was used for layer planarization. Next, two aluminum routing layers (M1 and M2) and vias were formed. Finally, edge coupler facets were formed by deep trench etching and the wafers were diced.

For device characterization, light was coupled onto the chips using cleaved single-mode optical fibers (Nufern S405-XP for visible light and Nufern 780-HP for λ=780nm). The fibers were aligned to edge couplers using piezo-actuated micromanipulators. We used a supercontinuum laser (NKT Photonics SuperK Fianium) with a tunable optical filter (NKT Photonics LLTF Contrast) as the light source. Optical transmission measurements of reference waveguides with nominally-identical edge couplers to the PD test structures were used to determine the optical power input to the PDs and to convert the photocurrent to responsivity. Electrical probing was performed using tungsten DC needles, and I-V characterization was conducted via a sourcemeter (Keysight B2912A Precision).

3. Photodetector Measurement Results

The characterization of our PIN SiN-on-SOI PDs on a representative chip is summarized in Fig. 2. The dark current for L_{PD}=200 μm was 3.4, 6.0, and 8.4 pA at reverse bias voltages of 2, 5, and 8V, respectively, Fig. 2(b). Measurements of two additional chips yielded similar results with dark currents < 8 pA at a 5V reverse bias. The PDs exhibited good linearity in their photocurrent response, which was linearly fitted with R^2 of 0.99 at 450 nm (Fig. 2(b), inset). The responsivity generally increased with PD length, Fig. 2(c), with the largest increases for λ = 488 and 640 nm and relatively small increases for λ=450 and 532 nm for L_{PD} > 50μm (indicating complete absorption at this length). This may be a consequence of the lower absorption of Si at longer wavelengths and possibly also modal hybridization enhancing absorption at 450 and 532 nm. The EQE for L_{PD}=200 μm is shown in Fig. 2(d). At λ = 450, 488, 532, and 640 nm, EQE > 70% and 35% was observed for the TE and TM polarizations, respectively. EQE measurements of two additional chips (limited to L_{PD}=200 μm and the TE polarization) agreed with Fig. 2(d) to within ±5%.

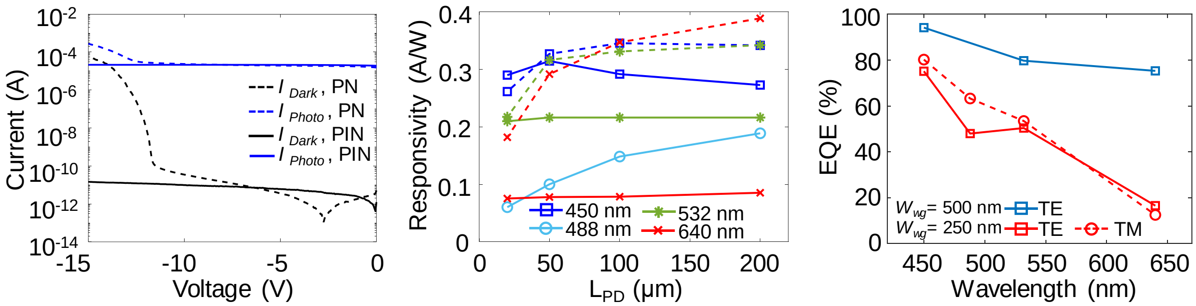

(a) (b) (c)

Fig. 3. PN PD characterization. (a) Comparison of I-V traces of PIN and PN PDs (W_{wg}=500nm, L_{PD}=200μm) with and without optical input (λ=450nm, TE-polarized, 60μW incident at the PD). (b) Responsivity vs. L_{PD} for PN PDs with TE-polarized optical inputs of various wavelengths; the solid lines correspond to PDs with W_{wg}=250nm, and the dashed lines correspond to PDs with W_{wg}=500nm. (c) EQE vs. wavelength (TE and TM) for 200μm-long PDs with W_{wg}=500nm and 250nm.

Additional responsivity and EQE measurements were performed in the NIR at λ = 780nm; however, a low EQE of 3.4% was observed. As the SiN waveguide dimensions were tailored to the VIS, optimal NIR performance is not expected here.

Our measurement results for PN SiN-on-SOI PDs on another representative chip are shown in Fig. 3. The PN PDs with L_{PD} = 200 μm exhibited a breakdown voltage of about -13V (Fig. 3(a)), while no breakdown was observed for corresponding PIN devices for reverse biases up to 15 V. Variations of the PN PDs with W_{wg} = 250 and 500 nm were investigated. The EQE for W_{wg}=250 nm was generally lower than for W_{wg}=500 nm, especially at longer wavelengths (Fig. 3(c)), and increasing L_{PD} was not an effective means of improving the performance (Fig. 3(b)). Overall, the EQE and dark current for the L_{PD} = 200 μm and W_{wg}=500 nm PN PD in Fig. 3 (EQE > 75% for the TE polarization, < 7 pA dark current at 5V reverse bias) were similar to that of the corresponding PIN PD in Fig. 2. However, the moderate breakdown voltage of the PN PD, Fig. 3(a), can potentially enable avalanche operation for low-light detection.

4. Conclusion

In summary, we have demonstrated broadband, high-efficiency, and low dark current SiN-on-SOI waveguide-coupled PDs in a foundry-fabricated visible-light integrated photonics platform. The PDs achieved EQE > 70% for TE-polarized red, green, and blue light, and the dark current was < 8 pA at a 5V reverse bias. Characterization of the electrical bandwidth and avalanche properties of the PDs is ongoing.

References

[1] W. D. Sacher et al., "Monolithically integrated multilayer silicon nitride-on-silicon waveguide platforms for 3-D photonic circuits and devices." Proceedings of the IEEE 106.12 2232-2245 (2018).
[2] E. Timurdogan et al., "AIM process design kit (AIMPDKv2. 0): Silicon photonics passive and active component libraries on a 300mm wafer," in OFC 2018.
[3] W. D. Sacher et al., "An Active Visible-Light Integrated Photonics Platform on 200-mm Si," in OFC 2023.
[4] C. Sorace-Agaskar et al., “Versatile silicon nitride and alumina integrated photonic platforms for the ultraviolet to short-wave infrared,” IEEE J. Sel. Top. Quantum Electron. 25, 1–15 (2019).
[5] N. F. Tyndall et al. "A Visible-Light Foundry Platform from AIM Photonics," in OFC 2023.
[6] A. Z. Subramanian et al., “Low-loss singlemode PECVD silicon nitride photonic wire waveguides for 532–900 nm wavelength window fabricated within a CMOS pilot line,” IEEE Photonics J. 5, 2202809 (2013).
[7] W. D. Sacher et al., "Visible-light silicon nitride waveguide devices and implantable neurophotonic probes on thinned 200 mm silicon wafers." Opt. Express 27.26 37400-37418 (2019).
[8] K. K. Mehta et al., "Integrated optical multi-ion quantum logic," Nature 586.7830 533-537 (2020).
[9] F. D. Chen et al., "Implantable neural probe system for patterned photostimulation and electrophysiology recording," in CLEO 2022.
[10] M. Raval et al., "Integrated visible light phased array system for autostereoscopic image projection," Opt. Lett. 43.15 (2018): 3678-3681.
[11] Z. Yong et al., "Power-efficient silicon nitride thermo-optic phase shifters for visible light," Opt. Express 30.5 7225-7237 (2022).
[12] M. Notaros, et al. "Integrated visible-light liquid-crystal-based phase modulators." Optics Express 30.8 13790-13801 (2022).
[13] M. Dong et al., "High-speed programmable photonic circuits in a cryogenically compatible, visible–near-infrared 200 mm CMOS architecture," Nat. Photon. 16.1 59-65 (2022).
[14] S. Yanikgonul et al., "Integrated avalanche photodetectors for visible light," Nat. Comm. 12.1 1834 (2021).
[15] Y. Lin et al., "Monolithically integrated, broadband, high-efficiency silicon nitride-on-silicon waveguide photodetectors in a visible-light integrated photonics platform." Nat. Comm. 13.1 6362 (2022).
[16] S. Cuyvers et al., "Heterogeneous integration of Si photodiodes on silicon nitride for near-visible light detection," Opt. Lett. 47.4 937-940 (2022).
[17] M. Corato-Zanarella et al., "Widely tunable and narrow-linewidth chip-scale lasers from near-ultraviolet to near-infrared wavelengths." Nat. Photon. 17.2 157-164 (2023).
[18] R. Morgan, et al., "Waveguide-integrated blue light detector." 2021 IEEE Photonics Conference (IPC). IEEE, 2021.